

Disorder induced hexagonal-orthorhombic transition in $\mathbf{Y}_{1-x}^{3+}\mathbf{Gd}_x^{3+}\mathbf{MnO}_3$

Jan-Willem G. Bos, Bas B. van Aken and Thomas T. M. Palstra

Solid State Chemistry Laboratory, Materials Science Centre, University of Groningen, Nijenborgh 4, 9747 AG Groningen, the Netherlands

(November 21, 2018)

We show that the transition in \mathbf{AMnO}_3 from the orthorhombic perovskite phase to the hexagonal phase is promoted by inducing disorder on the A-site. The gap between the orthorhombic and the hexagonal phase is widened for disordered, mixed yttrium-gadolinium manganite samples. At the cost of the orthorhombic phase a two phase region emerges. The phase separation exhibits very unusual thermodynamical behaviour. We also show that high pressure synthesis favours the orthorhombic phase. \mathbf{YMnO}_3 is formed in the orthorhombic phase at 15 kbar.

I. INTRODUCTION

In the search for new composition-properties relations \mathbf{ABO}_3 compounds have attracted a lot of attention. The perovskite materials, \mathbf{ABO}_3 , have been researched extensively because this structure forms the basis for interesting physical properties such as high T_c superconductivity [1] and colossal magnetoresistance [2]. Non-perovskite \mathbf{AMnO}_3 , with $\mathbf{A} = \mathbf{Y}, \mathbf{Ho}, \dots, \mathbf{Lu}$, attracted renewed interest, due to their ferroelectric properties [3]. These hexagonal \mathbf{AMnO}_3 [4] have a basically different structure than most \mathbf{ABO}_3 compounds, that are distorted perovskites. These properties arise due to the strong correlation of the $3d$ electrons with the $\mathbf{O} 2p$ orbitals.

In this paper, we report the transition from the orthorhombic perovskite (o) to the hexagonal (h) phase by changing the ionic radius of the A ion and by high pressure synthesis. The effect of the ionic radius on the transition is studied by partially replacing Y by Gd ions in \mathbf{YMnO}_3 . The resulting phase diagram leads us to discuss the effect of disorder, in terms of the ionic radius variance, on the stability of the hexagonal and orthorhombic phases.

The basic building block of the perovskite is an oxygen octahedron with a transition metal, B, in its centre. The A ions, usually lanthanides or alkaline earth metal ions, occupy the holes between the octahedra, that form a 3D corner shared network. In this picture B is sixfold and A is 12-fold coordinated. Most perovskites have a distorted structure, derived from this building block. The distortions have various origins, including a ferroelectric transition for B a d^0 transition metal ion like \mathbf{Ti}^{4+} [5]. The most common distortion originates from the relative small radius of the A ions compared with the holes between the octahedra. This results in a cooperative rotation of the octahedra known as the \mathbf{GdFeO}_3 distortion [6]. While the structure is interesting in its own right, it has also large effects on the physical properties. It is well documented that the physical properties depend strongly on the magnitude of the structural distortions. An overview for the manganites is given in Ref.'s [7,8].

The magnitude of the \mathbf{GdFeO}_3 distortion depends strongly on the tolerance factor, t :

$$t = \frac{r_{A^{3+}} + r_{O^{2-}}}{\sqrt{2}(r_{B^{3+}} + r_{O^{2-}})}, \quad (1)$$

where r_X is the radius of the X ion. The tolerance factor gives the relation between the radii of ions A, B and O in a ideal cubic perovskite. For $t = 1$ the size of the lanthanide is exactly right to compose the cubic perovskite system. For \mathbf{Mn}^{3+} , $r_{Mn^{3+}} = 0.645 \text{ \AA}$ and $r_{O^{2-}} = 1.42 \text{ \AA}$ this yields a ionic radius $r_{A^{3+}} = 1.50 \text{ \AA}$, where the largest lanthanide, La, has a radius of 1.22 \AA . The corresponding tolerance factor $t = 0.90$ indicates a large distortion for \mathbf{LaMnO}_3 . With increasing atomic number, the lanthanide radius decreases and thereby the distortion increases. For the manganites, the tolerance factor is conventionally regarded as the factor controlling the boundary between the hexagonal and orthorhombic structures. The orthorhombic perovskite phase is stable for $t > 0.855$, corresponding to $r_A \geq r_{Dy}$ [9]. For $t < 0.855$, $r_A \leq r_{Ho}$, the hexagonal phase prevails [4]. Yttrium, although not in the lanthanide series, behaves chemically identical and its radius falls between dysprosium and holmium. An overview on the ionic radii and tolerance factors of some relevant compounds is given in Table I.

TABLE I. Ionic radii and tolerance factors for relevant compounds.

Compound	tolerance factor	ionic radius (Å)
\mathbf{LaMnO}_3	0.902	1.215
\mathbf{GdMnO}_3	0.866	1.109
\mathbf{DyMnO}_3	0.857	1.083
\mathbf{YMnO}_3	0.854	1.075
\mathbf{LuMnO}_3	0.840	1.032

The high temperature phase of the hexagonal $AMnO_3$ consists of 8-fold coordinated A ions in bicapped antiprisms. Trigonal bipyramidal holes are formed between two layers of face-sharing antiprisms by the edges of the capping oxygens with the antiprisms. The capping oxygens of two adjacent layers are located on the same ab plane. Half of the bipyramidal holes are occupied by Mn. The apical oxygens of the MnO_5 bipyramid are also the oxygens that make up the antiprism. The two polyhedra are sketched in Fig. 1, where the shared edge is shown. The $Mn-O_{ap}$ distance is thus equal to the distance between the antiprism oxygen layer and the capping oxygen layer. The steric hindrance of the Mn restricts this layer separation and therefore increases the A-O_{ap} bond length. Thus, the eightfold co-ordination is not uniform. The two apical oxygens have slightly larger bond lengths. Furthermore, the structure is unstable against a ferroelectric distortion at lower temperatures. The apical oxygens move in such a way that one bond becomes 'normally' short, while the other becomes about 1 Å larger. The asymmetric A environment is the main reason for the ferroelectric behaviour. As we have two lanthanide positions in $P6_3cm$, we have two non-equivalent, although similar, dipole moments. Four out of the six moments per unit cell point upwards, the other two downwards.

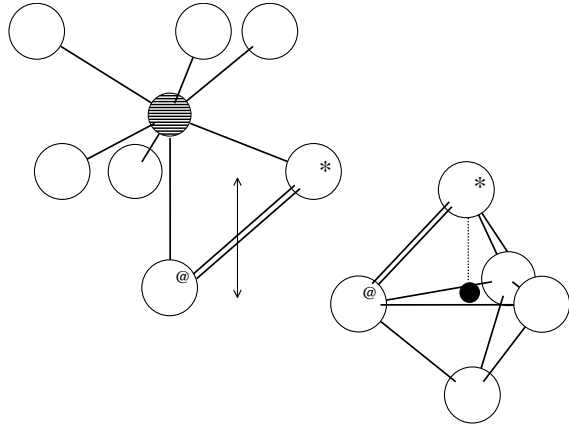


FIG. 1. Sketch view of the local environment, showing AO_7 , left side, and MnO_5 , right side. The arrow indicates the distance between two oxygen planes. The dashed line indicates the $Mn-O_{ap}$ distance. Atoms marked with "*" and with "@" are identical, the double line indicates the shared edge.

Although the hexagonal phase of $YMnO_3$ at ambient conditions is the thermodynamically stable phase, there are several ways to obtain orthorhombic $YMnO_3$. Using thin film growth, an appropriate substrate will force the coherent growth of the orthorhombic phase [10]. Synthesis routes via organic precursors and low reaction temperatures yield the orthorhombic phase [11]. And last, high pressure synthesis favours the orthorhombic phase, because it has a higher density [12].

II. EXPERIMENTAL

Polycrystalline ceramic samples of $AMnO_3$, where A is a mixture of Y and Gd, have been synthesised using regular solid state synthesis at ambient pressure. Starting materials were Y_2O_3 , Gd_2O_3 and MnO_2 . Stoichiometric amounts corresponding to formulae which range from pure $YMnO_3$ to pure $GdMnO_3$ were weighted and wet-mixed using acetone as liquid medium. The pressed pellets were sintered for 24 hours at 1250° and for 24 hours at 1400° .

High pressure experiments were carried out both on the mixture of oxides and on as-prepared samples. X-ray powder diffraction patterns were identical for both methods. The high pressure high temperature piston cylinder apparatus is a Depth of the Earth Quickpress 3.0, with an experimental range up to 25 kbar and 2100°C [13]. The lower pressure limit is ~ 1 to 2 kbar.

The sample environment is a complex set-up, including a graphite furnace and the pressure medium. Care has to be taken to prevent contamination from the graphite resistance furnace or any of the other materials, *e.g.* Al_2O_3 or $NaCl$, in the sample assembly. Therefore, a small amount of powder ~ 0.5 g was encapsulated in a Pt capsule. The capsule consisted of a tube (diameter 4 mm and height 6 mm) and two pre-shaped lids, which were welded together using a small welding apparatus. Recovery of the pellet from the sample assembly is improved by the Pt container.

X-ray diffraction patterns were recorded using a Bruker-AXS D8 powder diffractometer, with primary and secondary monochromator, using $Cu K_\alpha$ radiation. Patterns were analysed for phase determination using the evaluation software EVA [14], the Powder Diffraction File [15] and the Inorganic Crystal Structure Database [16]. Patterns of non-contaminated samples, containing only the hexagonal and orthorhombic phases, were used in the Rietveld refinement using TOPAS R [17]. Rietveld refinements included lattice parameters, zero point correction and the ratio between the two phases. Atomic positions were assumed to be constant using the positions determined by single crystal x-ray diffraction on $YMnO_3$ [18]. The ratio Y:Gd was fixed at the nominal composition.

TABLE II. Ionic radii, tolerance factors and variance of the studied $Y_{1-x}Gd_xMnO_3$ samples.

x	r_A (Å)	t	σ^2 (10^{-6} Å)
0	1.075	0.854	0
0.06	1.077	0.855	68
0.19	1.081	0.857	176
0.25	1.084	0.857	217
0.31	1.086	0.858	248
0.38	1.088	0.859	271
0.5	1.092	0.860	289
1	1.109	0.866	0

III. RESULTS AND DISCUSSION

In Fig. 2, we present a phase diagram of $\text{Y}_{1-x}\text{Gd}_x\text{MnO}_3$ as a function of r_A and its variance σ^2 of samples given in Table II. The variance σ^2 is given by,

$$\sigma^2 = \sum_1^n x_i(r_i - \langle r_A \rangle)^2 \quad (2)$$

The phase diagram can be divided in three regions. Low r_A compounds, $\langle r_A \rangle < 1.078$, are hexagonal. Large r_A and small σ^2 compounds are orthorhombic. The intermediate region shows both phases. The data for HoMnO_3 and DyMnO_3 have been taken from the literature [4].

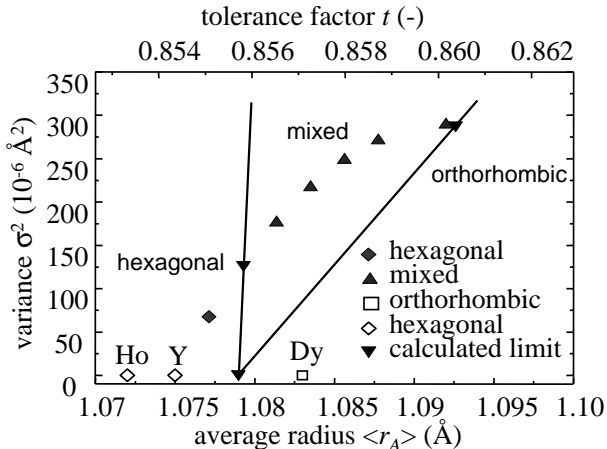


FIG. 2. Phase diagram of $\text{Y}_{1-x}\text{Gd}_x\text{MnO}_3$ as a function of r_A , or t , and the variance, σ^2 . Diamonds indicate hexagonal phase, triangles mixed phase and squares orthorhombic phase. The drawn lines are estimates of the phase boundaries as explained in the text. The end member GdMnO_3 has $r_A = 1.109 \text{ \AA}$.

By changing the value of x we substitute Y by Gd, whereby r_A increases linearly. The tolerance factor of orthorhombic DyMnO_3 is equal to that of $\text{Y}_{1-x}\text{Gd}_x\text{MnO}_3$, with $x = 0.23$. Thus for $x \gtrsim 0.23$ we expect to see the orthorhombic phase. For smaller x and t the hexagonal phase is expected. For $x = 0$ and $x = 0.06$ we indeed found the hexagonal structure. However, for $0.19 \leq x \leq 0.38$ we do not observe a sharp transition to the orthorhombic structure, but a mixture of the hexagonal and orthorhombic phases. Only for $x = 0.5$ an (almost) pure orthorhombic compound is found. The anomalous behaviour of the mixed Y,Gd samples is best illustrated by focussing on the sample with $x = 0.25$, which has an almost identical tolerance factor as DyMnO_3 . Where the latter sample is orthorhombic, the former segregates in both phases. The only difference between the two compounds is that one is undoped and the other has a mixed lanthanide composition.

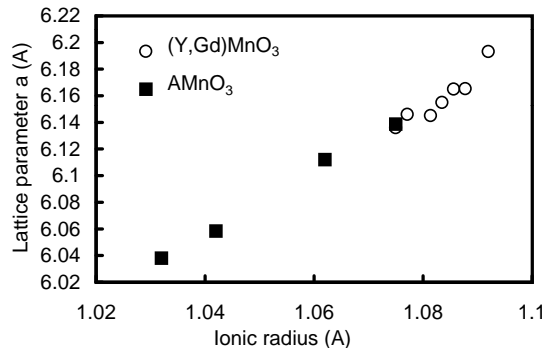


FIG. 3. Lattice parameter a of the hexagonal phase as a function of the Gd content x .

The relative amounts of orthorhombic and hexagonal fractions are determined by Rietveld refinement of the powder diffraction data, see Fig. 4. We can rule out element segregation of Y and Gd, since the continuous increase in the lattice parameter a of the hexagonal phase with increasing Gd concentration indicates perfect mixing of the A ions. A linear increase in a with r_A is also observed for the single A cation h-AMnO_3 series [4,18–20]. Fig. 4 shows that the orthorhombic phase fraction increases linearly with the Gd fraction. This allows us to apply the lever rule on the h-o transition

$$\frac{x - x_{\text{hexa}}}{x - x_{\text{ortho}}} = \frac{y_{\text{ortho}}}{y_{\text{hexa}}} \quad (3)$$

where x_{hexa} and x_{ortho} are the boundary values for the respective phases and $y_{\text{ortho}}/y_{\text{hexa}}$ the ratio of the two fractions. From the observed ratios $y_{\text{ortho}}/y_{\text{hexa}}$ as a function of x , the boundary values are derived. The boundary values derived from all five mixed phase samples are plotted in Fig. 2 as inverted triangles.

We construct a preliminary phase diagram by assuming that the h-o transition at $\sigma^2 = 0$ occurs halfway between hexagonal YMnO_3 and orthorhombic DyMnO_3 . The phase boundaries are drawn in Fig. 2 as straight lines through the two calculated boundary values and the assumed $\sigma^2 = 0$ midpoint. This phase diagram can be described as follows. The phase line associated with the upper t limit of the hexagonal phase does not depend on the variance. Slightly increasing σ^2 and t results in the appearance of a two phase region, consisting of both the hexagonal and the orthorhombic phase. With increasing tolerance factor, the fraction of the orthorhombic phase increases until the lower boundary limit for the orthorhombic phase is crossed. This limit strongly depends on σ^2 . The lower limit for the orthorhombic phase increases from $r_A = 1.078 \text{ \AA}$ at $\sigma^2 = 0$ to $r_A = 1.093 \text{ \AA}$ at $\sigma^2 = \sigma_{\text{max}}^2$. Note that $r_A = 1.093 \text{ \AA}$ corresponds with the ionic radius of terbium, the second smallest lanthanide to form the perovskite structure.

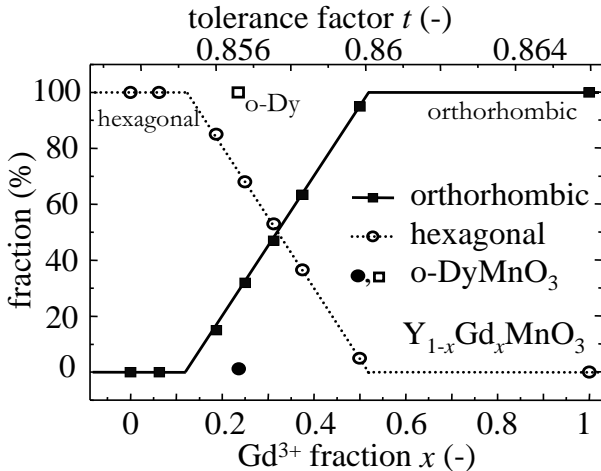


FIG. 4. Relative amounts of hexagonal, triangles, and orthorhombic, squares, fractions as a function of the Gd content x . An open square is plotted for DyMnO_3 at the corresponding value of the tolerance factor.

We have shown the dependence of the h-o transition on the average radius r_A and σ^2 . In the next section, the effect of high pressure experiments on the h-o transition will be discussed.

We applied high pressure and high temperature to convert or synthesise some of the conventionally hexagonal samples in the orthorhombic state. Pressure generally stabilises the most dense phase, in this case the orthorhombic structure. First, we consider samples with $\sigma^2 = 0$. YMnO_3 is still hexagonal at 5 kbar, but the orthorhombic phase is found using a pressure of 15 kbar. The data is shown in Fig. 5. The necessary pressure for the h-o transition, less than 15 kbar, is much less than reported previously in the literature [12]. The h-o transition phase line has been sketched in Fig. 5 by using midpoints. Extrapolating the pressure dependence of the h-o transition yields a critical pressure of $\lesssim 27$ kbar for HoMnO_3 . The error bar on this value, ~ 10 kbar, is large because of the sparse data points.

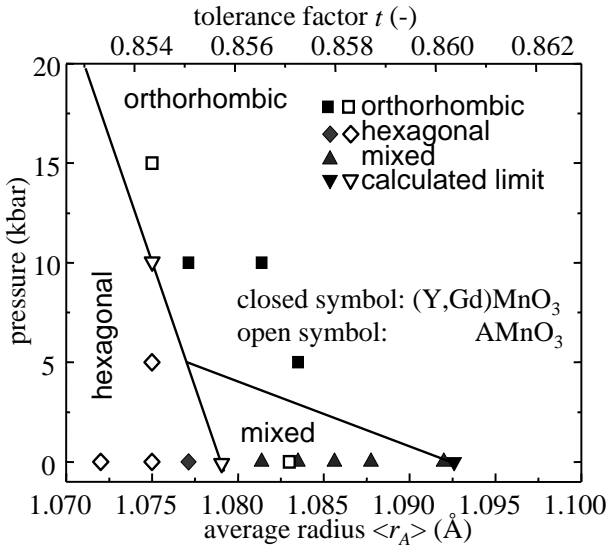


FIG. 5. Pressure versus average radius phase diagram. Undoped samples are shown with open symbols, doped Y-Gd samples with closed symbols. We never observed mixed samples after high pressure synthesis. Schematic phase boundaries are drawn.

We also carried out high pressure experiments on the $\text{Y}_{1-x}\text{Gd}_x\text{MnO}_3$ compounds. The necessary pressure to induce the orthorhombic phase from the phase mixture decreased with increasing r_A .

We note the following observations of the two-phase region:

1. The phase mixture is only observed for ambient pressure synthesis for samples with $\sigma^2 \neq 0$.
2. We do not observe the mixed phase for any of the experiments at high pressure (≥ 5 kbar). We cannot exclude the presence of the mixed phase at low pressures, but our experimental set-up is not well-suited for those pressures.
3. The lattice parameters of both phases in the two phase region indicate no segregation into Y-rich and Gd-rich phases, see Fig. 3, which is unconventional.
4. Literature reports that synthesis via organic precursors can result in a mixture of hexagonal and orthorhombic phases for AMnO_3 , $\sigma^2 = 0$, compounds [11].

These observations lead to the following conclusions. For $\sigma^2 = 0$ compounds either the hexagonal or the orthorhombic structure is stable. Whereas low temperature synthesis may yield mixed phase samples, a high temperature anneal will convert the unstable phase. The hexagonal or orthorhombic phase will be stable depending on the tolerance factor. However for $\sigma^2 \neq 0$ mixed phase samples can be obtained for a broad range of tolerance factors. Even a high temperature anneal retains the phase segregated state. Surprisingly, the phase segregation is not accompanied by two limiting compositions, e.g. $\text{Y}_{1-x}\text{Gd}_x\text{MnO}_3$ with $x = 0.1$ and $x = 0.5$. The continuous increase of the lattice parameters of both the hexagonal and the orthorhombic phase throughout the two phase region indicates that the composition of the hexagonal and the orthorhombic state are the same in the mixed state. We have no explanation for this unconventional form of phase segregation.

IV. CONCLUSIONS

We have constructed phase diagrams for the h-o phases of AMnO_3 , including the effects of average ionic radius, hydrostatic pressure and variance. For compounds with $\sigma^2 \neq 0$ a phase separation in the orthorhombic and the

hexagonal phase is found. The mixed region exists only at low pressures. We have shown that at ambient pressure, this region expands towards higher values of the average radius with increasing variance. The upper limit for the hexagonal phase is not affected by an increase in the variance. We speculate that disorder, introduced by a large variance or soft chemical synthesis routes, allows the occurrence of the phase separation in the absence of other driving forces. Suppressing the disorder by applying external pressure or annealing at high temperatures prevents the existence of the phase separation. Pressure favours the denser, orthorhombic phase, whereas thermal annealing promotes the hexagonal phase.

This work is supported by the Netherlands Foundation for the Fundamental Research on Matter. (FOM).

- [1] J. G. Bednorz and K. A. Muller, *Z. Phys. B* **64**, 189 (1986).
- [2] S. Jin *et al.*, *Science* **264**, 413 (1994).
- [3] E. F. Bertaut, E. F. Forrat, and P. Fang, *C. R. Acad. Sci.* **256**, 1958 (1963).
- [4] H. L. Yakel *et al.*, *Acta Cryst.* **16**, 957 (1963).
- [5] A. von Hippel *et al.*, *Ind. Eng. Chem.* **38**, 1097 (1946).
- [6] A. M. Glazer, *Acta Cryst.* **B28**, 3384 (1972).
- [7] A. P. Ramirez, *J. Phys.: Cond. Mat.* **9**, 8171 (1997).
- [8] J. M. D. Coey, M. Viret, and S. Von Molnar, *Adv. Phys.* **48**, 167 (1999).
- [9] H. L. Yakel, *Acta Cryst.* **8**, 394 (1955).
- [10] P. A. Salvador *et al.*, *Chem. Mater.* **10**, 2595 (1998).
- [11] H. W. Brinks, H. Fjellvåg, and A. Kjekshus, *J. Solid State Chem.* **129**, 334 (1997).
- [12] A. Waiental and J. Chenavas, *Mat. Res. Bul.* **2**, 819 (1967).
- [13] *Quickpress 3.0 piston cylinder apparatus, operations manual* (Depths of the Earth Company, 738 S. Perry lane, Tempe, Az, USA).
- [14] EVA 4.0, Bruker AXS, software program, 1998.
- [15] Powder Diffraction File, NIST, Database, 1998.
- [16] Inorganic Crystal Structure Database, Fachinformationsszentrum Karlsruhe, Germany, 2001.
- [17] TOPAS 2.0, Bruker AXS, Software program, 2000.
- [18] B. B. Van Aken, A. Meetsma, and T. T. M. Palstra, *Acta Cryst.* **C57**, 230 (2001).
- [19] B. B. Van Aken, A. Meetsma, and T. T. M. Palstra, *Acta Cryst.* **E57**, i38 (2001).
- [20] B. B. Van Aken, A. Meetsma, and T. T. M. Palstra, Single crystal structure determination of YbMnO_3 and LuMnO_3 , unpublished results, 2000.